J. Fluid Mech. (2000), *vol.* 403, *pp.* 133–151. Printed in the United Kingdom

On the influence of centrifugal buoyancy on rotating convection

By J. E. HART

Program in Atmospheric and Oceanic Sciences, University of Colorado, Boulder, CO 80309, USA

(Received 15 December 1998 and in revised form 26 August 1999)

Centrifugal buoyancy forces in a container rotating about an axis aligned with gravity lead to mean flows that interact with rotating convection. A model of the interactions between these flows and the thermal instabilities that occur in weakly nonlinear rapidly rotating convection is used to estimate when, in terms of external parameters, centrifugal buoyancy has a substantial influence on thermal convective instability. The significant physical effects include the direct action of centrifugal buoyancy on the eddies themselves, the upwards advection of basic-state vertical shear by the perturbation rolls, and the alteration of the mean thermal stratification upon which eddies grow by the basic centrifugally induced circulation. It is shown that the first effect is the most important for common laboratory settings, and can lead to destabilization of the system at outer radii. Other manifestations of centrifugal buoyancy include the generation of a positive offset of the mean temperature at the centre of the cell, and a reduction of this offset by heat fluxes arising from the centrifugally modified finite-amplitude convective eddies.

1. Introduction

There has been renewed interest in the properties of thermal convection in rapidly rotating systems. Recent studies include direct numerical simulation (Julien *et al.* 1996), LES computations (Klinger & Marshall 1995), semi-analytic modelling (Julien & Knobloch 1998) and a number of experimental studies (Boubnov & Golitsyn 1990; Fernando, Chen & Boyer 1991; Sakai 1997; Liu & Ecke 1997), amongst many others. Recent experiments in our own laboratory (Hart & Ohlsen 1999, hereafter referred to as HO99) have shown that high Rayleigh number rapidly rotating convection exhibits an offset in the mid-depth mean temperature such that the centrepoint value is above the average of the bounding horizontal plates. In addition, the mid-depth eddy variance is higher near the outside of the tank than at the axis (Liu & Ecke 1998; HO99). In an early work on the onset of rotating convection, Koshmeider (1967) found that axisymmetric rings in a high Prandtl number fluid first appeared near the outer regions of the cylindrical test cell as the Rayleigh number was increased past its critical value. What could account for this offset, the rim amplification in supercritical systems, and rim preference for first appearance of convective instabilities? In the modelling work and in the interpretation of experiments, centrifugal buoyancy, which is always present to some degree in rotating convection systems, is usually neglected.

In order to illustrate the interactions between rotating convection and centrifugal buoyancy-induced motions in the simplest possible analytical model, a weakly nonlinear formulation for convection at rapid rotation rate is developed. Although it is not rigorously feasible to address turbulent convection experimental results with this approach, having a tractable model that can at least suggest trends as the eddy amplitude increases is useful and appealing. The model is based on the classical Rayleigh–Bénard situation in which the flow is bounded above and below by two rigid large-diameter discs maintained at a temperature difference ΔT. In summary, the questions asked are:

(i) What is the direct centrifugal circulation that is driven by centrifugal buoyancy acting on the conduction gradient? Does the centrifugal circulation lead to a mean thermal offset at the midpoint of the layer? To complete the instability analysis, the centrifugally induced motion needs to be computed to second order in an amplitude expansion that introduces some nonlinearity to the mean meridional cell.

(ii) As the relative strength of the centrifugal-buoyancy circulation is increased, when does it first affect the basic instability of rotating convection? Is the system more or less stable than the canonical conductive situation with a no-motion, vertical-gravity basic state? What are the physical mechanisms that cause the instability to be either suppressed or enhanced?

(iii) How does the eddy heat flux through the layer change as centrifugal buoyancy is added to the problem? Does it compensate or enhance the mean thermal offset in the layer that is associated with the mean cell?

Question (ii) was considered in the theoretical calculations of Homsy & Hudson (1971). Their theory predicts changes in the critical Rayleigh number for convection in the presence of a centrifugal-buoyancy circulation in a finite cylinder of radius L. This circulation is composed of a self-similar interior and a two-dimensional (non-self-similar) rim flow. The former stabilizes convection while the latter is found to be destabilizing. The parameter values for which their asymptotic analysis applies are somewhat removed from typical terrestrial experimental values. For example, the Froude number $\Omega^2 L/g$ is assumed large (see further discussion in §2). In addition, their stability computation focuses on how the changes to the basic-state thermal stratification associated with the centrifugally induced mean flow affect convective instability. They neglect the direct consequences of centrifugal-buoyancy forces arising from eddy temperature fluctuations. Our analysis indicates that for typical laboratory settings this assumption is likely to be invalid. A simple physical interpretation for the destabilization of convection by this direct centrifugal action is offered.

The paper is organized as follows. A model for the mean circulation is introduced and solved in §2. Second-order finite-amplitude solutions are obtained that are later used in the weakly nonlinear stability calculation of §3. This calculation hinges on assuming a large Taylor number where the order of the vertical structure problem is reduced to two, and the nonlinear cascade is much more easily carried out than if one had to use the full rigid-wall eigenfunctions at each step. In Appendix B it is shown, asymptotically, how the instabilities of the classical rotating Rayleigh–Bénard problem with rigid no-slip conditions at the horizontal bounding surfaces approach the reduced (free-boundary) solutions as the Taylor number Ta is increased. The results of the weakly nonlinear analysis and their implications are summarized in §4.

2. The circulation induced by centrifugal buoyancy

Consider the motion between two infinite discs a distance H apart. The discs are infinitely conducting and are maintained at a temperature difference ΔT. They are oriented perpendicular to gravity and rotate at rate Ω. The non-dimensional Boussinesq equations of motion for axisymmetric flow relative to the conductive temperature profile are

$$u_t + \boldsymbol{u} \cdot \nabla u = -p_r + (v^2/r + v)Ta + (\nabla^2 u - u/r^2) - Ta\Gamma r[-z + PrT], \quad (1a)$$

$$v_t + \boldsymbol{u} \cdot \nabla v = -(uv/r + u) + (\nabla^2 v - v/r^2), \quad (1b)$$

$$w_t + \boldsymbol{u} \cdot \nabla w = -p_z + \nabla^2 w + RaT, \quad (1c)$$

$$Pr[T_t + \boldsymbol{u} \cdot \nabla T] = w + \nabla^2 T, \quad (1d)$$

$$u_r + u/r + w_z = 0, \quad (1e)$$

where the parameters in the above equations are

$$Ra = g\alpha\Delta T H^3/\kappa\nu, \quad (2a)$$

$$Ta = 4\Omega^2 H^3/\nu^2, \quad (2b)$$

$$Pr = \nu/\kappa, \quad (2c)$$

$$\Gamma = \alpha\Delta T/4. \quad (2d)$$

The parameters for the infinite disc problem are the Rayleigh, Taylor, Prandtl, and density deficit numbers, respectively. In a general problem of flow in a finite cylinder of radius L, additional parameters of importance are the Froude number

$$F = \Omega^2 L/g,$$

and the aspect ratio

$$\gamma = L/H.$$

Note that the gravitational buoyancy appears in the last term on the right of (1*c*), while the centrifugal buoyancy, acting on the total temperature field, is contained in the bracketed term on the right of (1*a*). The neglect of centrifugal buoyancy is sometimes based on the smallness of F, and results in the omission of the bracketed term from (1*a*). Previous studies of rotating stratified flows (e.g. Barcilon & Pedlosky 1967; Homsy & Hudson 1969) have shown that F is not necessarily the correct parameter to measure the relative significance of centrifugal accelerations.

The scales used to get (1) are H (length), ν/H (u and w), $2\Omega H(v)$, and H^2/ν (time). Here u is the radial velocity, v is the azimuthal velocity, and w is the vertical velocity, while p is the non-dimensional fluctuating pressure normalized by the mean density ρ_0. In the Boussinesq approximation there is a static pressure field quadratic in r and linear in z that balances the gravitational and centrifugal accelerations of fluid having this mean density. In (1) and (2) α is the coefficient of expansion, ν the kinematic viscosity, H the layer depth, Ω the rotation rate (anti-parallel to the gravity g), κ the thermal diffusivity, and ΔT the applied temperature difference. The dimensional temperature field, taken to be statically unstable if $\Delta T > 0$, is given by

$$T^* = \Delta T[-z^*/H + PrT(r, z, t)]. \quad (3)$$

It is first necessary to derive a second-order solution giving the steady mean centrifugal circulation. Homsy & Hudson (1971) use asymptotic methods to arrive at a basic centrifugal flow near a sidewall, and this near-wall analysis is restricted by the condition that $\gamma\Gamma PrTa^{1/4}/F \ll 1$. In Koshmeider's (1967) experiments, representing normal terrestrial laboratory conditions, although Γ is very small, Pr is very large, so for his moderately large aspect ratio (10), fairly large Taylor number (100), and moderately small Froude number $F\,(\sim 0.1)$, this parameter group is in fact quite large (>100). To find the near-sidewall circulation for typical terrestrial laboratory conditions where F is small it appears necessary to turn to fully nonlinear two-dimensional computational simulation. While this is certainly feasible, the present goal of constructing a relatively simple theoretical model motivates us to concentrate on the region of a shallow container that is located of order H units in from the cylinder rim. Simulations of the fully nonlinear problem in a cylinder with various sidewall thermal conditions show that for typical parameter settings a slow circulation with a simple self-similar spatial structure can indeed exist over the bulk of the region (Brummell, Hart & Lopez 1999). Thus we confine our analysis to the inner 80% to 90% of the radius in a cylinder with a large aspect ratio γ. In this region the basic state has a relatively simple shape which is now obtained.

Following Duncan (1966) and Hudson (1968) a similarity reduction for steady motion between parallel infinite discs is employed by writing

$$T = T_c(z), \quad u = rU_c(z), \quad v = rV_c(z), \quad w = W_c(z), \quad p = P_c(z) + r^2 TaP_b/2. \tag{4}$$

This transformation of (1) results in

$$U_c^2 + W_cU_c' = (V_c^2 + V_c)Ta + U_c'' - \Gamma\, Ta(-z + PrT_c) - TaP_b, \tag{5a}$$

$$U_cV_c + W_cV_c' = -(U_cV_c + U_c) + V_c'', \tag{5b}$$

$$PrW_cT_c' = T_c'' + W_c, \tag{5c}$$

$$2U_c = -W_c'. \tag{5d}$$

The z-dependent part of the pressure field $P(z)$ is passive in this problem, and can be determined from the vertical balance $P_c' = W_c'' + RaT_c - W_cW_c'$ once the vertical velocity and temperature fields are found. Equations (5), as well as (1), are subject to homogeneous boundary conditions on the three velocity components and the temperature that are applied at $z = \pm 1/2$:

$$U_c = V_c = W_c = T_c = 0 \quad \text{at } z = \pm 1/2. \tag{5e}$$

The system (5*a*)–(5*d*) is seventh order, but the addition of a barotropic radial pressure field, proportional to the constant P_b, permits the eight boundary conditions to be imposed.

As we are interested in finding out when centrifugal buoyancy first influences rotating convection, and this is presumed to happen when the centrifugal circulation is weak, it is sufficient to obtain the linear solution to (5), along with the first nonlinear correction to it. In linearizing (5) the physical assumption is that the actual temperature perturbation PrT_c is small compared with that of the conductive thermal distribution, and that rotation is sufficiently large that $Ta > 1$. This, along with the fact that $\Gamma \ll 1$ for typical liquids, guarantees that V, hence U and W, will also be small. In this situation the linear centrifugal circulation is governed by

$$U_c'' + V_cTa = -\Gamma\, Taz, \tag{6a}$$

$$U_c = V_c'', \tag{6b}$$

$$T_c''' = W_c' = 2U_c = 2V_c''. \tag{6c}$$

The barotropic pressure correction P_b is not needed at lowest order because we can find a solution that is antisymmetric about the origin and so therefore satisfies mass balance automatically with $P_b = 0$. Equations (6) describe a mean circulation that

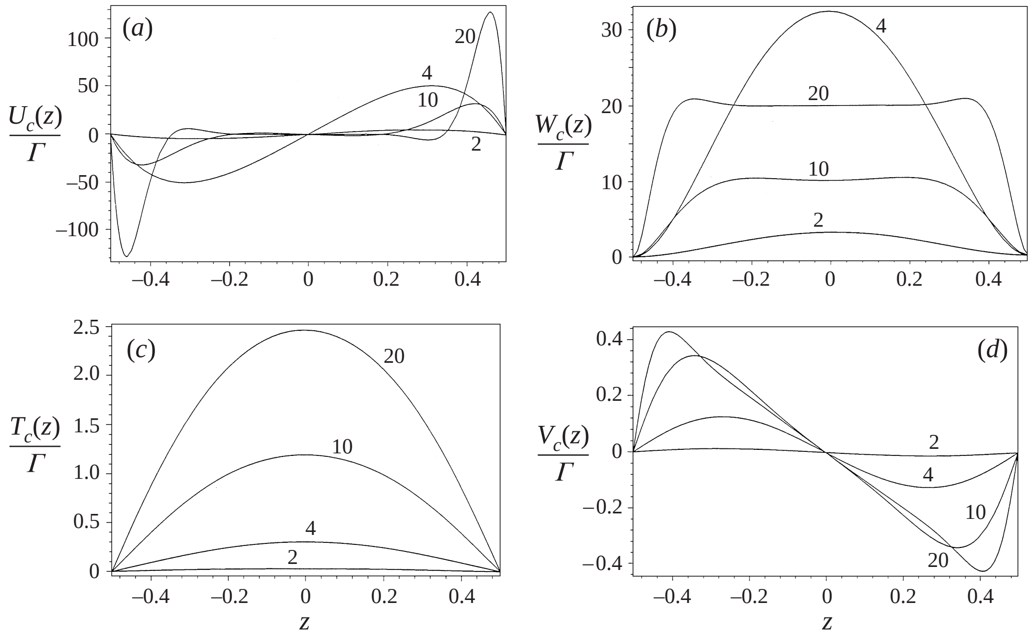

FIGURE 1. Characteristics of the linear centrifugal buoyancy circulation. Velocities and temperature, normalized by Γ, are shown for $\eta = 2$, 4, 10 and 20. (a) Normalized radial velocity, curves for $\eta = 2$ and 4 are multiplied by 10; (b) normalized vertical velocity, curves for $\eta = 2$ and 4 are multiplied by 10; (c) normalized temperature fluctuation T (see (3)); (d) normalized azimuthal velocity.

consists of radial outflow in the top half of the layer, with inflow in the lower half. This leads to a vertical circulation in the inner bulk of the layer which is upwards. Once V and U are determined, T and W are found by simple integration using (6c). All the fields are proportional to Γ. The solutions are given in Appendix A in terms of the inverse non-dimensional Ekman layer thickness that we define by

$$\eta \equiv (Ta/4)^{1/4}. \tag{7}$$

Figure 1 illustrates the evolution of linearized flow with increasing η. It agrees with the numerical solutions of the ODE system (5) by Hudson (1968). At large Taylor number the radial solution collapses into two Ekman layers attached to the discs. There is only azimuthal motion in the interior, where the horizontal Coriolis acceleration acting on the azimuthal velocity balances the radial centrifugal buoyancy acceleration. For our purposes we note that the thermal perturbation at moderately large Taylor number responds to the almost uniform vertical velocity in a manner that generates a parabolic temperature distribution at large η. Therefore, outside the thin Ekman layers attached to the two plates, the centrifugal circulation for $\eta \gg 1$ takes on a compact form: T is parabolic, W is constant, and V is linear in z. Thus we can write, with the subscript 1 denoting the linear solution in the interior:

$$W_c \equiv W_{c1} = W_c(0), \tag{8a}$$

$$U_c \equiv U_{c1} = 0, \tag{8b}$$

$$T_c \equiv T_{c1} = 4T_c(0)(1/4 - z^2), \tag{8c}$$

$$V_c \equiv V_{c1} = -\Gamma z. \tag{8d}$$

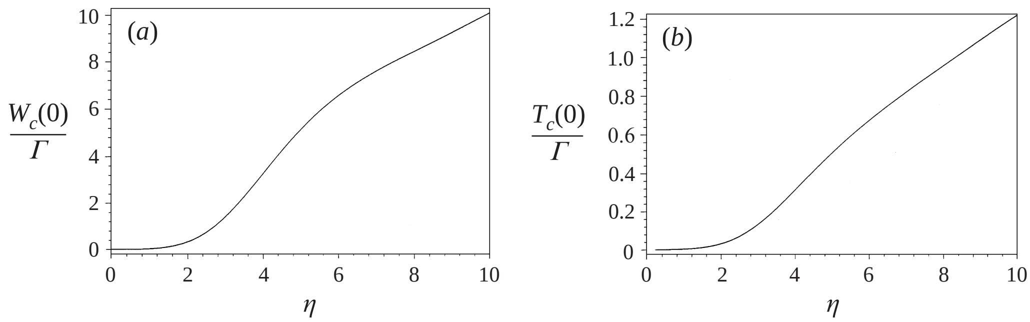

FIGURE 2. Dependence of the linear solution (*a*) vertical velocity and (*b*) core temperature on η at the mid-plane $z = 0$.

Figure 2 illustrates how the mid-plane vertical velocity and temperature vary in general with η. These are given by

$$W_c(0) = -\Gamma\eta \frac{e^{-\eta} + 2e^{-\eta/2}\sin(\eta/2) - 1}{e^{-\eta} + 2e^{-\eta/2} + 1}, \tag{9a}$$

$$T_c(0) = -\frac{\Gamma}{8\eta}\{-8e^{-3\eta/2}(\cos(\eta/2) + \sin(\eta/2)) + 2\sin(\eta)e^{-\eta}(4 + \eta^2) + (4 - \eta^2)e^{-2\eta} \\ +8e^{-\eta/2}(\cos(\eta/2) - \sin(\eta/2)) - 4 + \eta^2\}/\{(4\cos^2(\eta/2) - 2)e^{-\eta} - 1 - e^{-2\eta}\}. \tag{9b}$$

The dependence of both $W_c(0)$ and $T_c(0)$ on η becomes linear somewhat beyond the point where the representation (8) starts to be accurate in the interior. In particular,

$$T_c(0) \to \eta/8 \quad \text{and} \quad W_c(0) \to \eta, \tag{10}$$

when η is greater than about $6\,(Ta \geqslant 5000)$, giving, via (8*a*–*d*), a quite simple description of the motion. For example, the thermal perturbation scales with $Pr\Gamma\eta/8$, relative to the conductive background profile.

The first nonlinear correction to these interior flows is required for the stability calculation of § 3. Fortunately it is not necessary to iterate about the full solutions given in Appendix A because the finite-amplitude analysis only needs the interior solution. The boundary layers (here the $Ta^{-1/4}$-thick Ekman layers), do not significantly affect the stability problem when the Taylor number is large. The second-order interior flow is driven by the nonlinear terms in (5) that are evaluated by substituting from (8). In the interior these forcings excite second-order motions whose horizontal velocities are reduced to zero at the wall by attaching the appropriate linear Ekman layers. The result for the interior motion is

$$V_{c2} = -\Gamma^2 z^2 + \Gamma^2 Pr\eta(1/4 - z^2)/2 + P_b, \tag{11a}$$

$$P_b = \Gamma^2[17/20 - 3/2\eta + 1/\eta^2 + Pr(1/2\eta - 1/2)], \tag{11b}$$

$$U_{c2} = \Gamma^2[\eta(1 - Pr) - 2], \tag{11c}$$

$$W_{c2} = -2\Gamma^2[\eta(1 - Pr) - 2]z, \tag{11d}$$

$$T_{c2} = -\Gamma^2[\eta^2 Pr/6 + \eta(Pr - 1)/3 + 2/3](z^3 - z/4). \tag{11e}$$

To conserve mass in the presence of the depth-independent interior radial motion described by (11*c*) an equal amount of fluid must move radially in the opposite direction in the top and bottom Ekman layers. A radial pressure gradient is needed to generate this radial motion in the boundary layers. This pressure gradient is in turn associated with a depth-independent solid rotation that is reflected in the last term on the right of (11*a*). The magnitude of the barotropic pressure gradient P_b is found by matching the Ekman suction just outside the boundary layers at $z = \pm 1/2$ to (11*d*). The Ekman pumping velocity is in part a result of reducing the horizontal velocities (11*a*) and (11*b*) to zero at the walls. However, we also need to include the antisymmetric contribution to the boundary layer pumping due to the nonlinear interactions in the first-order boundary layers themselves. This arises because the linear centrifugal interior solution (8) has a cyclone near the lower boundary and an anticyclone near the upper plate. The lowest-order boundary layer velocities associated with these interior motions advects fluid inside the boundary layers in a manner that generates changes in the net suction. Using the model of Hart (1995), nonlinear corrections to the lowest-order Ekman suction associated with (8*d*) are included in the determination of P_b.

The dominant (at large η) part of the second-order azimuthal velocity derives from the centrifugal buoyancy arising from the thermal field in (8*c*). The barotropic swirl associated with P_b turns out to be fairly small. As opposed to the linear solution (8) where T and W are about the same size, the second-order solution is dominated by temperature corrections (11*e*) at large Taylor number. This will have important consequences for our stability analysis. Under these conditions the centrifugally induced thermal field $Pr\,(T_{c1} + T_{c2})$ is the most important of the basic-state variables in altering the criticality condition for convection. While the first-order solution (8*c*) has increased static stability near the upper boundary and an equivalent decrease of static stability near the bottom, the second-order temperature gradient obtained from (11*e*) is even in z with a positive value at the midplane (for $Pr > 1$).

Use of the 'infinite disc' solutions given by (8) and (11) in practical applications assumes that the meridional circulation described above, with uniform upflow, is passively connected to a return circulation flowing down in a thin boundary layer at the inevitable sidewall. Previous studies of similar problems (Barcilon & Pedlosky 1967; Homsy & Hudson 1969) suggest that this centrifugal circulation will be closed at the sidewall with a Stewartson inner layer of thickness $E^{1/3} \approx \eta^{-2/3}$, where E is the Ekman number. Instead of (6*c*), the sidewall thermal field is determined by $\nabla^2 T \approx T_{rr} = -w(z, (r_0 - r)\eta^{2/3})$, where w is the sidewall boundary layer component of the vertical velocity. For an insulating sidewall it can be shown that no homogeneous solution of $\nabla^2 T = 0$ (which would have roughly equal horizontal and vertical variations) is required, because the particular solution of $T_{rr} \approx -w$ satisfies the wall condition $\partial T/\partial r = 0$ directly. Similar comments apply to the sidewall layers attached to (11).

3. Finite-amplitude rapidly rotating convection with centrifugal buoyancy

For near-critical flows, the Rayleigh number is written as

$$Ra = Ra_c(1 + \varepsilon), \tag{12}$$

where Ra_c is the critical Rayleigh number for convection in the absence of centrifugal mean flows (basically the free–free critical curve, see Appendix B), and $\varepsilon \ll 1$ represents the supercriticality. In the presence of centrifugal buoyancy, ε may be non-zero at neutrality, reflecting the alteration of the critical curve by centrifugal effects. An amplitude equation is obtained in the standard way by iterating the partial differential equation for the fluctuating streamfunction using the weakly nonlinear cascade procedure. At large Taylor number the disturbance horizontal scales are small compared with the distance required for significant variation of the basic state (in r). For example, it is well known that the most unstable convective instabilities under fast rotation have small horizontal scale (proportional to $Ta^{-1/6}H$). The centrifugal circulation is broad, varying at most with scale H. We choose a location (in r) and consider the fate of rectilinear disturbances on the combined conductive/centrifugal basic state. A local analysis that takes place in the vicinity of a base radius $x_s = r$ is used. For simplicity, only longitudinal modes (e.g. axisymmetric modes) are studied. The vertical shear in the azimuthal component of the centrifugal flow (figure 1d) is expected to force alignment of eddies into the azimuthal (y) direction. The fundamental equations are obtained by expressing the local radial and vertical velocities in terms of the streamfunction $\psi : u = -\psi_z,\ w = \psi_x$. The azimuthal velocity in the local y-direction, v, is also assumed to be a function of the deviation from the base radius, x, and the height z. The locally rectilinear two-dimensional fully nonlinear model is

$$
\begin{aligned}
&Ta\psi_{zz} - Ra_c\psi_{xx} + \psi_{xxxxxx} \\
&\quad = Ra_c\varepsilon\psi_{xx} + \nabla^2\{\nabla^2\psi_t + \psi_x\psi_{xxz} - \psi_z\psi_{xxx} + w_c\psi_{xxz} + u_c\psi_{xxx} - x\Gamma\, TaPrT_z\} \\
&\quad\quad -PrRa_c\frac{\partial}{\partial x}\{T_t + \psi_x T_z - \psi_z T_x + w_c T_z + u_c T_x + \psi_x T_{cz}\} \\
&\quad\quad +Ta\frac{\partial}{\partial z}\{v_t + \psi_x v_z - \psi_z v_x + w_c v_z + u_c v_x + \psi_x v_{cz} - \psi_z v_{cx}\},
\end{aligned}
\tag{13a}
$$

along with

$$\nabla^2 T + \psi_x = Pr[T_t + \psi_x T_z - \psi_z T_x + w_c T_z + u_c T_x + \psi_x T_{cz}], \tag{13b}$$

$$\nabla^2 v + \psi_z = [v_t + \psi_x v_z - \psi_z v_x + w_c v_z + u_c v_x + \psi_x v_{cz} - \psi_z v_{cx}], \tag{13c}$$

where

$$\nabla^2 = \partial^2/\partial z^2 + \partial^2/\partial x^2.$$

Equation (13a) is obtained by combining the two-dimensional vorticity equation (for the $\hat{y}$-vorticity) with the thermal and azimuthal velocity equations. To make the problem analytically tractable, (13a) has been reduced using the fact that the convection cells are tall and thin at high Taylor number. One result of this simplification is that $\partial^2/\partial x^2 \gg \partial^2/\partial z^2$ so that the operator $\nabla^6\psi$, which would normally appear on the left of (13a), is replaced by ψ_{xxxxxx}. The forcing terms on the right of (13a) are similarly reduced. This narrow-cell approximation effectively reduces the differential order of the problem in height from sixth to second. As a result, the solutions to equations (12) are required to satisfy $\psi = \overline{T} = \bar{v}_z = 0$ at $z = \pm 1/2$, where the overbar denotes the mean-field corrections. This reduction of order enormously simplifies the algebra involved in explicitly computing the nonlinear cascade. Further commentary on this approximation appears in Appendix B, which indicates the Taylor number values for which rigorous equivalence of the full rigid wall and the reduced problems is expected. Equations (13b) and (13c) are the two-dimensional thermal advection–diffusion equation and the $\hat{y}$-velocity (i.e. the azimuthal velocity) equation respectively. They are used to find the temperature and azimuthal velocity fields once the streamfunction is determined from (13a). In (13) the motion has been decomposed into a sum of the known centrifugal circulation, with subscript c, and the convective motions that are to be found (not subscripted). In the following calculation we consider the most common laboratory situations with Prandtl number greater than unity and focus, for simplicity, on stationary modes of instability. The convection field is expanded as

$$\psi = |\varepsilon|^{1/2}\psi_1 + |\varepsilon|\psi_2 + |\varepsilon|^{3/2}\psi_3 \ldots, \tag{14}$$

with similar representations for T and v. The centrifugal circulation is inserted into the calculation using (3), (8), and (11). It is assumed that $\Gamma \approx O(|\varepsilon|^{1/2})$. This order-of-magnitude relation implies that the centrifugal circulation will interact with the convection at second order in powers of $|\varepsilon|^{1/2}$. Also important is the observation that the lowest-order convection mode ψ_1 is even in z, and so interacts with the odd centrifugal V and the even centrifugal W and T to produce an odd ψ_2. When this latter field (and its associated temperature perturbation and swirl velocity) interacts with the lowest-order centrifugal circulation, and when ψ_1 interacts with the second-order centrifugal mean flow, resonances arise. Removal of these resonances, carried out in practice by multiplying the order-$\varepsilon^{3/2}$ version of (13*a*) by ψ_1 and integrating over a wave period in x and across the layer in z, leads to a nonlinear ordinary differential equation for the amplitude $A(t)$ of the lowest-order solution ψ_1.

One twist to this familiar procedure is that the x-integration takes place over a cycle of the basic eigenfunction, but offset from the origin by an amount x_s. This is required because the horizontal velocity components of the centrifugal mean flows increase linearly with 'radius' x, and different positions may be expected to give different coefficients in the amplitude equations. Indeed, the linear increase of centrifugal acceleration with radius, as well as the linear increase of the azimuthal component of centrifugal buoyancy circulation with radius, are both important physical effects that must be retained. These x-variations mean that the stability problem is no longer translation invariant. Thus the amplitude equation will not have the normal Landau form. In particular, it will have an A^2 term in addition to the usual A and A^3 terms.

The computations, though algebraically involved, were successfully carried out using the computer-algebra program MAPLE. The lowest-order problem gives the linear solution: $\psi_1 = A(\tau)\cos(\pi z)\sin(kx)$, $T_1 = A(\tau)\cos(\pi z)\cos(kz)/k$, $v_1 = -A(\tau)\pi\sin(\pi z)$ $\sin(kx)/k^2$, where k is the radial wavenumber of the convection unmodified by centrifugal effects. By Appendix B this is just k_f, the free–free critical wavenumber. The second-order solution is driven by interactions between the linear centrifugal circulation and the linear convection mode, and by the convection mode with itself. The resulting fields (ψ_2, T_2, v_2) are quite complicated, though analytically determined. These are used to compute the interactions between the first-order motions (convection and centrifugal, e.g. $\psi_1+\psi_{c1}$) and the second-order flows (convection plus centrifugal, e.g. $\psi_2+\psi_{c2}$). Multiplying these forcing terms, which appear in the order-$\varepsilon^{3/2}$ problem from (13*a*), by $\psi_1/A(\tau)$, and then integrating this over the gap between the plates and from $x = x_s$ to $x_s + 2\pi/k$, finally yields the amplitude equation for centrifugally modified longitudinal modes of rotating convection. This amplitude equation is

$$\mathrm{d}A/\mathrm{d}\tau = \{(17.822\,\mathrm{sgn}(\varepsilon) + C_1)A + C_2A^2 - (2.227Pr^2 - 8.609Ta^{-1/3})A^3\}, \tag{15}$$

where $\tau \equiv Ta^{1/3}|\varepsilon|(10.46Pr - 3.49)t$. The numeric constants reflect the values of the projection integrals in the resonance removal algorithm. The signs are important. Since we are investigating $Pr > 1$ and large-Ta situations, it is seen, for example, that the instability is supercritical. Equation (15) is consistent with the models of Veronis (1966, 1968) who found steady subcritical instability in pure gravitational rotating convection, but only at very low Prandtl number.

The coefficients C_1 and C_2 are discussed in Appendix C. In general they vary with the basic radius (measured in units of the layer depth) x_s. However, the leading asymptotic approximation to C_1 as $Ta \rightarrow \infty$ is independent of x_s. It is

$$C_1 \approx \frac{\Gamma^2}{|\varepsilon|}[-0.0809 Pr^2 Ta^{1/2} + O(Ta^{1/4})]. \tag{16}$$

C_2 varies with x_s in its leading term. The magnitude of C_2 is only $\Gamma/\sqrt{|\varepsilon|}Ta^{1/6}$. At large Taylor number the effect of the quadradic term in (15) in thus negligible. In this situation the dominant terms in (15) are independent of x_s (provided the limit $Ta \rightarrow \infty$ with x_s fixed is taken).

One goal of the analysis is to determine the effect of centrifugal buoyancy on the linear stability of rotating thermal convection. Equation (15) can now be used to determine the actual linear critical point, including centrifugal effects, because small-amplitude neutrality requires $17.822\,\mathrm{sgn}(\varepsilon) + C_1 = 0$. Using the leading term in (16) gives

$$\Gamma^2 Pr^2 Ta^{1/2} = 220\varepsilon, \tag{17}$$

which shows that the centrifugal solution makes the motion more stable ($\varepsilon > 0$). In practice, if we expect an experiment to observe the critical point to within 1%, then the centrifugal circulation first becomes significant when $\alpha\Delta T Pr Ta^{1/4} \approx 6$.

What is the physical origin of the negative sign of (15)? Term by term inspection reveals that this value is set by vertical advection of the centrifugal temperature field by the convective eddy. There are two competing contributions. The interaction between $w_2 = \psi_{2x}$ and T_{c1z} is destabilizing. This is expected as it is known that an antisymmetric change in the basic stratification (more unstable near one wall, more stable near the other, see (8*c*)) renders the linear convective mode more unstable. However, the interaction between ψ_{1x} and T_{c2z} does the opposite. T_{c2z} is stable (positive) in the interior where the convective vertical velocity is large. On the other hand where T_{c2z} is unstable (negative) near the walls, the convective vertical velocity w goes to zero. Thus the $\psi_{1x}T_{c2z}$ interaction is stabilizing, and turns out to be larger in magnitude than the destabilizing effect of the $\psi_{2x}T_{c1z}$ interaction. This leads to the net stabilization expressed in (17). This stabilization of convection by the centrifugal mean thermal field is in accord with the findings of Homsy & Hudson (1971).

However, although $\alpha\Delta T Pr Ta^{1/4}$ is the parameter that asymptotically measures the effect of centrifugal buoyancy on rapidly rotating convection when Ta is large, it may not be the practically relevant one. This is because the asymptotic series for C_1 has a numerically large term multiplying a slightly lower power of Taylor number. This term (see Appendix C) will dominate in most practical situations where $1 \ll Ta \ll [6(Pr-1)L/HPr]^{12}$. For example, if the apparatus is 10 height units wide, large Prandtl number disturbances occurring near the rim at $x_s = 10$ will feel this latter term first unless $Ta > O(10^{18})$. Thus, a more practical estimate of the linear neutral curve is obtained by the alternative approximation introduced in Appendix C:

$$C_1 \approx \frac{\Gamma^2}{|\varepsilon|} x_s^2 Ta^{1/3}(Pr-1)^2/2. \tag{18}$$

In this circumstance the neutrality condition gives

$$\Gamma^2(Pr-1)^2 Ta^{1/3} \approx -\frac{35.6\varepsilon}{x_s^2}. \tag{19}$$

Note that for this slightly restricted Taylor number range the centrifugal motion now destabilizes the system ($\varepsilon < 0$). Equation (19) suggests that the centrifugal buoyancy

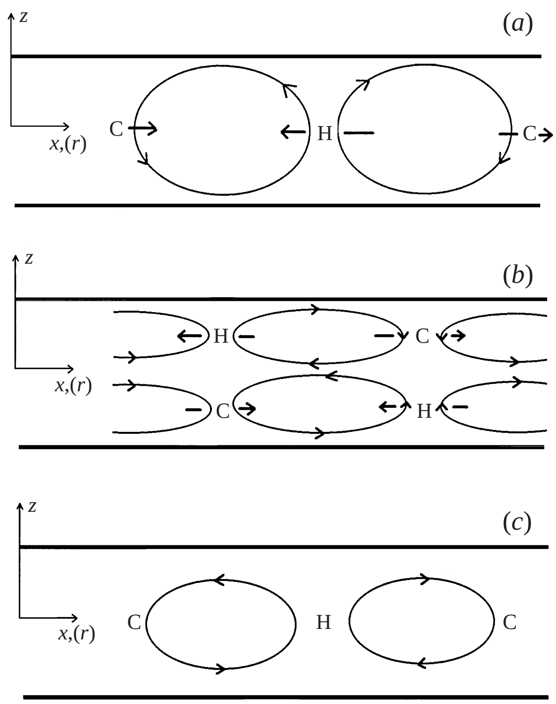

FIGURE 3. Sketches of convection in the radius–height plane. (*a*) The lowest-order ψ_1 convection roll that is unmodified by centrifugal buoyancy. Location of hot (H) and cold (C) thermal perturbations are shown, along with bold arrows that indicate the directions of the centrifugal buoyancy forces acting on fluid with these temperatures. (*b*) The second-order ψ_2 field that would arise by driving associated with the centrifugal buoyancy forces in (*a*), and the net radial centrifugal buoyancy forces acting on the T_2 fields that occur by advection of the statically unstable basic conductive state via ψ_2. (*c*) The component of the circulation induced by the centrifugal buoyancy forces in (*b*).

will first influence convection near the rim of the apparatus, and a 1% shift in the neutral curve will arise when $\varepsilon = 0.01$, or when $\alpha\Delta T(Pr-1)Ta^{1/6}L/H \approx 2.3$. For example, if the aspect ratio and the Prandtl number are both about 10, and $Ta = 10^6$, then centrifugal buoyancy will affect the convection if $\alpha\Delta T >\approx 0.002$. In a silicone oil where $\alpha = 0.001$, a temperature difference of a degree or two will lead to recognizable centrifugal effects on the onset of convection. In Koshmeider's (1967) experiments $\alpha\Delta T(Pr-1)Ta^{1/6}L/H \approx 40$. Although his $Ta \sim 80$ is probably not sufficient to justify use of the reduced form (13*a*), nor the use of the asymptotic forms (8) and (11) for the centrifugal circulation, this theory suggests a possible mechanism to explain his observations of first appearance of axisymmetric instabilities near the rim of the container as ΔT is raised.

What physically causes this theoretical destabilization? Figure 3(*a*) illustrates the lowest-order roll circulation. It is unaffected by centrifugal buoyancy. The upwelling increases the mid-plane temperature between the two rolls shown via vertical advection of the conductive gradient. There is a radial (x-directed) buoyancy force that now acts on this temperature distribution, leading to the second-order circulation as sketched in figure 3(*b*). This circulation is orthogonal to, or does not reinforce, the basic cells in (*a*). Its magnitude scales with $x_s\Gamma PrTa^{1/6}$. Centrifugal buoyancy acts on the second-order temperature field generated by vertical advection within these cells, leading to a third-order circulation (figure 3*b*) that does project onto (i.e. is resonant with)

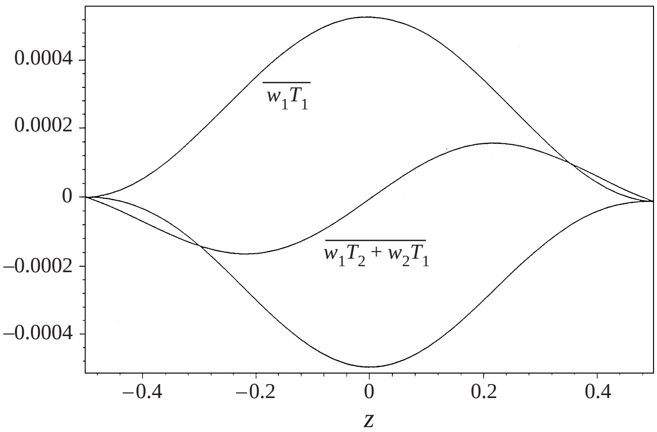

FIGURE 4. Characteristic eddy heat fluxes and the forced third-order mean temperature field for $\epsilon = 0.1$, $\Gamma = 0.001$, $Ta = 10^8$, $Pr = 10$, $x_s = 4$.

and indeed reinforces the basic cells of figure 3(a). The third-order cell amplitude scales with $(x_s\Gamma Pr)^2 Ta^{1/3}$. This net fortification leads to a reduction in the critical Rayleigh number that is proportional to $x_s^2\Gamma^2 Pr^2 Ta^{1/3}$. In (19), the factor $Pr - 1$ appears instead of Pr alone because eddy vertical advection of centrifugal azimuthal velocity leads to Coriolis accelerations that compete with the above mechanism. The appearance of unity in this factor is a result of the special spatial structures associated with the lowest order free–free solutions. For rigid boundaries this factor would be different, but for large Pr (19) is likely to remain accurate. It is useful to note that this effect is relatively independent of the mean centrifugal circulation (8) and (11), since it reflects the direct action on the eddies which in our ordering of the problem feel the mean flow at second and higher orders. For example, the first action takes the lowest-order pure gravitational rolls and perturbs them according to figure 3(b).

Using the analytic forms generated in the analysis, it is possible to calculate the contributions to the mean (x-averaged over 1 cell period at radius x_s) heat flux $\overline{wT}$. These may be divided into the purely convective second-order eddy part $\overline{w_1T_1}$, uninfluenced by centrifugal buoyancy, and the third-order term $F_3 = \overline{w_2T_1 + w_1T_2 + W_{c1}\overline{T_2} + W_{c2}T_{c1} + W_{c1}T_{c2}}$, which drives a third-order mean temperature field via $T_{3zz} = PrF_{3z} - W_{c3}$. The terms that make up this latter flux represent self-interactions in the eddy field, products of the centrifugal circulation and the nonlinear mean thermal field, and interactions between the centrifugal circulation and itself. For a wide range of parameters (all that were tested), all five terms are negative for $z < 0$ and positive for $z > 0$. For $\varepsilon \approx 0.1$, $\Gamma \leqslant\approx 0.001$, $Pr = O(1\text{–}20)$, $10^3 < Ta < 10^8$, being typical experimental values, the second term in F is the biggest. This indicates that unless the Taylor number or Γ are unusually large, the heat flux is dominated by the convective eddies. A typical distribution of the flux and the induced third-order temperature is illustrated in figure 4. Note that the lowest-order pure gravitational eddies will heat the top of the layer and cool the bottom, but will not alter the mid-plane temperature. The first convective–centrifugal buoyancy interaction will cool the mid-plane mean temperature and thus well compete with the result from § 2 that the direct action of centrifugal buoyancy on the conductive thermal field will be to produce a heating of the mid-plane.

Combining all these effects, and using an equilibration amplitude that is obtained

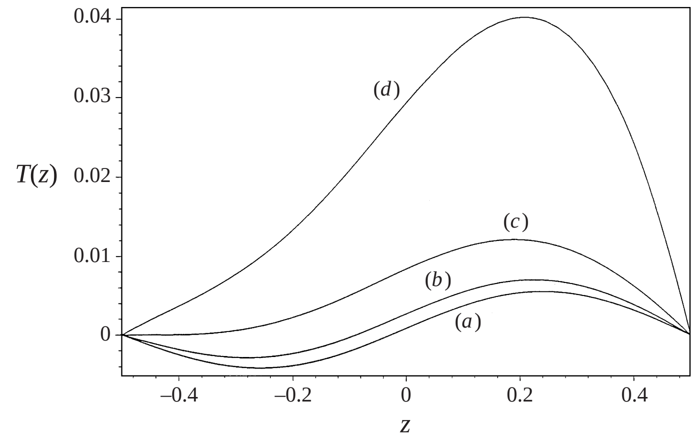

FIGURE 5. Mean (eddy-cell-averaged) temperature (not including the basic conductive gradient) for $x_s = 1$, $Pr = 10$, and $\epsilon = 0.1$. (*a*) $\Gamma = 0.0001$, $Ta = 10^8$; (*b*) $\Gamma = 0.001$, $Ta = 10^6$; (*c*) $\Gamma = 0.001$, $Ta = 10^8$; (*d*) $\Gamma = 0.005$, $Ta = 10^8$.

from (15) with $\dot{A} = C_2 = 0$, the central core temperature at large Taylor number is given by

$$\overline{T(x = z = 0)} = 0.088\Gamma Ta^{1/4} - 0.286\Gamma Ta^{1/4}\varepsilon/Pr - 0.01\Gamma^3 Pr(Pr-1)Ta^{1/2} + 0.00092Pr^2\Gamma^3 Ta^{3/4} + \Gamma^3 Pr^2 Ta^{1/2}/192. \quad (20)$$

The terms independent of ε represent offsets generated by the weakly nonlinear mean meridional centrifugal flow by itself. The last term in (20), which is not included in figure 4, gives the contribution due to advection of the conductive basic-state gradient by W_{c3}. This latter quantity is obtained by iterating the interior centrifugal circulation once again following the method used to get (8) and (11). Equation (20) illustrates explicitly the tendency for centrifugal buoyancy to directly induce a thermal offset at the cell mid-point, and for convection, via the second term on the right, to decrease this positive offset. Finally, figure 5 shows several typical distributions of mean temperature near the axis for moderate Prandtl number. The role of centrifugal buoyancy in contributing to the apparent asymmetry about the mid-plane is clearly evident as Γ or Ta get large.

4. Conclusions

This paper illustrates several aspects of how centrifugal buoyancy influences rapidly rotating convection between parallel differentially heated plates.

1. Centrifugal buoyancy acting on the linear (statically unstable) conductive temperature profile generates a ‘centrifugal mean circulation’. This consists of a single meridional cell with core upwelling, outflow of cold fluid in the top half of the layer, inflow in the bottom half, and an asymmetric (in the weakly nonlinear case) thermal profile. This direct circulation is accompanied by a positive thermal offset at the centre of the layer. Such offsets have been observed in experiments (Liu & Ecke 1998; HO99).

2. The analysis of the stability problem for rotating convection between parallel discs in the presence of mean circulations induced by centrifugal buoyancy shows that:

(a) The lowest-order centrifugal mean thermal field, which enhances the unstable basic-state conductive gradient near the upper plate and reduces it near the lower plate, tends to make the combined mean state more unstable.

(b) The second-order (slightly nonlinear) centrifugal mean thermal field, which is statically stable in the interior, tends to make the whole system more stable.

The detailed calculation shows that (b) is more important, so the lowest vertical critical mode of stationary convection is stabilized by the centrifugal circulation. At extremely large Taylor number this is the dominant physical effect. In this situation the convection will be stabilized by centrifugal buoyancy, and the degree of stabilization will be independent of radius. This result is similar to that obtained by Homsy & Hudson (1971) for the region away from the sidewall of their model configuration.

However, if the Taylor number is in the range $1 \ll Ta \ll [6(Pr-1)L/HPr]^{12}$, then the stabilization of convection by the vertical thermal gradient in the centrifugal cell is not the dominant effect. Rather, at the outer radii of a finite container, the direct action of centrifugal buoyancy on the convective eddies themselves will destabilize the convection in the sense that the critical Rayleigh number will be lowered. It is suggested that this mechanism may be an alternative to that proposed to act near the rim of a high Froude number system by Homsy & Hudson (1971), whose analysis concentrates on the interaction of convection with centrifugally modified mean temperature fields. They neglect the direct centrifugal buoyancy forces within the convection perturbations. Our destabilization mechanism results in a slow modulation of the eddy heat flux with radius which increases with $x_s^2 = r^2$, along with a similar radial increase of the basic eddy amplitude and thermal variance. Measurements of thermal variances in turbulent convection (Liu & Ecke 1998; HO99) show enhancement of these variables as a temperature probe is moved from the axis towards the sidewall that suggest such spatial modulation.

3. Analysis of the eddy correlations shows that those heat fluxes due to the interaction of the convection with the centrifugal buoyancy tend to carry heat out of the centre of the layer towards the horizontal plates. Therefore convection may moderate the positive thermal offset generated by the lowest-order centrifugal circulation itself through its core upwelling. It has been noted by HO99 that the direct centrifugal offset (e.g. (8c) or figure 2(b), calculated with a suitably renormalized basic gradient appropriate for strongly turbulent convection) overestimates that observed in turbulent rotating convection. Although suggested by a weakly nonlinear theory and perhaps not applicable to strongly supercritical convection, the tendency for finite-amplitude convection to reduce the mid-plane temperature offers a possible explanation.

As already, noted, laboratory experiments may exceed the threshold for centrifugal influence in the linear problem, $C \equiv \alpha\Delta T\, Pr\, Ta^{1/6}L/H \approx O(1)$. This is certainly true in Koshmeider's (1967) experiments. However these may not have had large enough Taylor number for the present analysis to apply. In our own unit-aspect-ratio highly turbulent experiments with a low-viscosity silicone oil, we have $\alpha\Delta T \approx 0.03, Pr \approx 10$, and $Ta \approx 10^8$, so that the above parameter is about 5. Although several features such as increased eddy amplitudes at large radii are common to both existing experiments and this model, it would be interesting to conduct experiments that better meet the constraints of the theory, namely moderate supercriticality, high Taylor number, large aspect ratio. It is probably difficult to get a large Taylor number if the Pandtl number is large. An alternative and potentially fruitful approach would be to carry out two-dimensional computational simultations in a high-aspect-ratio geometry at modest Prandtl number. Diagnosis of the resulting flow fields should be able to distinguish between the direct action of eddy centrifugal-buoyancy forces, proposed here as a destabilizing effect (i.e. an eddy energy source), and other mechanisms, such as the interaction between convective eddies and the mean centrifugally induced stratification changes near the rim.

This research was sponsored by the National Science Foundation, Division of Atmospheric Sciences, under grant ATM-97-14221 to the University of Colorado, and by support from NASA through its Microgravity Research Program, grant NAG-3-1848. I thank Patrick Weidman and the anonymous referees for helpful comments.

Appendix A. The linear centrifugal-buoyancy circulation

The formulae below give the solutions to the lowest-order (linear) problem (6) with homogeneous boundary conditions on all four variables at $z = \pm 1/2$. In the following let $\theta_{\pm m} \equiv m\eta/2 \pm \eta z$:

$$V_{c1} = -\Gamma z - \Gamma \frac{-\mathrm{e}^{\theta_{-3}} \cos\theta_{+1} + \mathrm{e}^{\theta_{-1}} \cos\theta_{-1} + \mathrm{e}^{\theta_{+3}} \cos\theta_{-1} - \mathrm{e}^{\theta_{+1}} \cos\theta_{+1}}{4\mathrm{e}^{\eta} \cos\eta - 2\mathrm{e}^{2\eta} - 2}, \tag{A 1}$$

$$U_{c1} = \Gamma \eta^2 \frac{-\mathrm{e}^{\theta_{-1}} \sin\theta_{-1} + \mathrm{e}^{\theta_{+1}} \sin\theta_{+1} - \mathrm{e}^{\theta_{-3}} \sin\theta_{+1} + \mathrm{e}^{\theta_{+3}} \sin\theta_{-1}}{1 - 2\mathrm{e}^{\eta} \cos\eta + \mathrm{e}^{2\eta}}, \tag{A 2}$$

$$\begin{aligned} W_{c1} = \Gamma \eta \{ & 1 + \mathrm{e}^{\theta_{+3}} \cos\theta_{-1} - \mathrm{e}^{\theta_{+1}} \cos\theta_{+1} - \mathrm{e}^{\theta_{-1}} \cos\theta_{-1} + \mathrm{e}^{\theta_{+3}} \sin\theta_{-1} + \mathrm{e}^{\theta_{-3}} \sin\theta_{+1} \\ & + \mathrm{e}^{\theta_{+1}} \sin\theta_{+1} + \mathrm{e}^{\theta_{-1}} \sin\theta_{-1} + \mathrm{e}^{\theta_{-3}} \cos\theta_{+1} - 2\mathrm{e}^{\eta} \sin\eta - \mathrm{e}^{2\eta}\} / \{2\mathrm{e}^{\eta} \cos\eta - \mathrm{e}^{2\eta} - 1\}, \end{aligned} \tag{A 3}$$

$$\begin{aligned} T_{c1} = \Gamma \{ & -4 - 8\mathrm{e}^{\eta} \sin\eta + 4\mathrm{e}^{\theta_{-3}}(\sin\theta_{+1} - \cos\theta_{+1}) + 4\mathrm{e}^{\theta_{-1}}(\sin\theta_{-1} + \cos\theta_{-1}) \\ & + 4\mathrm{e}^{\theta_{+3}}(\sin\theta_{-1} - \cos\theta_{-1}) + 4\mathrm{e}^{\theta_{+1}}(\sin\theta_{+1} + \cos\theta_{+1}) + 4\mathrm{e}^{2\eta} - 4\eta^2 z^2 + \eta^2 \\ & + 8\eta^2(z^2 - \eta^2/4)\mathrm{e}^{\eta} \sin\eta + 4\eta^2 \mathrm{e}^{2\eta}(z^2 - 1/4)\} / \{16\eta \mathrm{e}^{\eta} \cos\eta - 8\eta \mathrm{e}^{2\eta} - 8\eta\}. \end{aligned} \tag{A 4}$$

Appendix B. Asymptotic analysis of the rigid-boundary linear stability problem

The goal of this paper is to calculate a weakly nonlinear amplitude equation for rapidly rotating thermal instabilities in the presence of the centrifugally induced circulation described above. In order to simplify the calculations to the point where analytical methods are sufficient, it is useful to demonstrate how the normal rigid wall rotating convection problem asymptotically approaches a simpler problem governed by a vertical-structure differential equation with reduced order. In the paragraphs below, asymptotic relations are derived that show how the boundary layers that arise near $z = \pm 1/2$ in the rigid wall problem actually affect the neutral curves. By direct analysis Chandrasekhar (1961) shows that the rigid-boundary linear critical curve runs below and seemingly parallel to the classical free-boundary neutral curve for large Ta (values up to 10^{10} were shown). As $Ta \to \infty$ the boundary layer correction appears to vanish so the rigid–rigid and free–free critical curves come together. Julien & Knobloch (1998) argue that under such circumstances the requisite boundary layers near rigid plates must be passive, and the interior motions will behave as if the boundaries are free. It is useful to indicate how fast this happens. We do this by analysing the standard rotating convection stability problem for stationary two-dimensional perturbations by explicitly breaking up the solution into interior and boundary layer parts and by comparing solutions obtained with full rigid-wall boundary conditions with solutions from reduced (essentially free–free) boundary conditions.

Linear instabilities of gravitational convection are formally governed by the equation obtained by setting the right-hand side of (13*a*) to zero and returning to the full diffusion operator:

$$\nabla^6\psi - Ra\psi_{xx} + Ta\psi_{zz} = 0, \tag{B 1}$$

where ψ is the streamfunction for perturbations in the (x, z)-plane, with x chosen arbitrarily here to increase in the r-direction. Substituting $\psi = G(z)\sin kx$ leads to the standard sixth-order ODE, with $\mathrm{D} = \mathrm{d}/\mathrm{d}z$, for the linear eigenfunctions of rotating convection:

$$\underset{\text{(bl)}}{\mathrm{D}^6G} - \underset{\text{(bl)}}{3k^2\,\mathrm{D}^4G} + 3k^4\,\mathrm{D}^2G - \underset{\text{(int)}}{k^6G} + \underset{\text{(int)}}{k^2RaG} + \underset{\text{(bl, int)}}{Ta\,\mathrm{D}^2G} = 0. \tag{B 2}$$

Assuming Ra and k scale approximately with the free–free values $Ta^{2/3}$ and $Ta^{1/6}$ respectively, which will be the case if rigid walls have a small effect on the free–free neutral curve, then the balances shown under (B 2) permit calculation of the interior (int) and boundary layer (bl) motions with residual relative errors of order $Ta^{-1/3}$.

The solution, looking at the lowest vertical mode, and assigning unit amplitude to the interior streamfunction, is given by

$$G(z) = \cos lz + b\,\mathrm{e}^{-\eta(1+3k^2/\sqrt{Ta})(z+1/2)}\sin\eta(1-3k^2/\sqrt{Ta})(z+1/2)$$
$$+c\mathrm{e}^{-\eta(1+3k^2/\sqrt{Ta})(z+1/2)}\cos\eta(1-3k^2/\sqrt{Ta})(z+1/2), \tag{B 3}$$

where b and c are constants to be determined, and

$$l = \sqrt{\frac{Rak^2 - k^6}{Ta}}. \tag{B 4}$$

For compactness of presentation only the boundary layer at the lower plate is included explicitly in (B 3). Since the streamfunction is even, the structure near the upper plate is easily obtained from that shown above. The thermal perturbation is $T = [F(z)+d\exp(-k(z+1/2))]\cos(kx)$, where $F(z)$ is found by solving, to at least the same level of accuracy as above, the linearized thermal equation $\nabla^2T = -\psi_x$ using (B 3). Here d is a last undetermined constant. The total solution consists of an order-one varying interior (since l is order one), with modified Ekman layers and a $Ta^{-1/6}$ thermal layer lying near the plates. The three rigid-wall infinitely conducting boundary conditions $G = G' = T = 0$ at $z = -1/2$ serve to determine b, c, and d. Integration of the uniformly valid version of the vorticity equation $\nabla^4\psi + RaT_x - Tav_z = 0$ across the layer, and applying the boundary condition $v(\pm 1/2) = 0$, provides a fourth constraint. Using the thermal equation to relate the integral of T to G, and to the wall gradients of temperature, this procedure yields, with relative error of order $Ta^{-1/4}$,

$$G''(-1/2) + (Ra - k^4)\sin(l/2)/l + Ra\,\mathrm{D}T(-1/2)/k = 0. \tag{B 5}$$

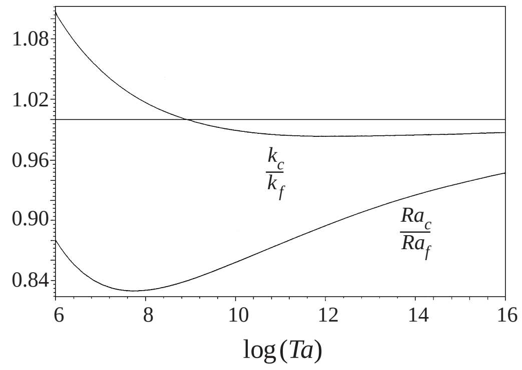

FIGURE 6. Asymptotic rigid-boundary critical Rayleigh number and wavenumber, normalized by the asymptotic free boundary values.

Using (B 3), the related vertical structure function for T, and the expressions for b, c, and d, we obtain a transcendental equation $\chi(l, Ra, Ta, k) = 0$ for the neutral curve. Solution of this eigenvalue problem using (B 4) is carried out with the symbolic manipulator MAPLE in the limit $Ta \to \infty$. The dominant terms are

$$Ra_c = Ra_f[1 - 1.107Ta^{-1/12} + 0.00001Ta^{-1/6} + 5.847Ta^{-1/4} + 4.549Ta^{-1/3}\ldots], \tag{B 6}$$

$$k_c = k_f[1 - 0.2768Ta^{-1/12} + 0.9966Ta^{-1/6} + 3.0011Ta^{-1/4}\ldots], \tag{B 7}$$

where

$$Ra_f = 3\pi^{4/3}2^{-2/3}Ta^{2/3}, \tag{B 8}$$

$$k_f = \pi^{1/3}2^{-1/6}Ta^{1/6} \tag{B 9}$$

are the critical points for the pure interior-only problem from (B 2) in which the single condition $G = 0$ is imposed on the first term in (B 3). These latter values, as well as the associated eigenfunction $\psi = \cos(lz) \to \cos(\pi z)$, are in fact equivalent to the asymptotic (large-Ta) results for the free–free boundary problem. Equations (B 6) and (B 7) show that the rigid boundary case is more unstable than the free case. This happens because the phasing is such that Ekman pumping adds constructively to the interior vertical velocity, thereby permitting the rigid mode to more effectively extract energy out of the basic conductive state than can the free mode. The rigid case approaches the free case slowly (like $Ta^{-1/12}$), and at moderate Taylor number some of the other terms in (B 6) and (B 7) are numerically significant. The result of the asymptotic analysis is shown graphically in figure 6. Over the entire range of Ta in figure 6 the differences between the full and reduced solutions are less than 15%, and asymptotically go to zero as $Ta \to \infty$.

The bottom line is that the use of the interior balance in (B 2), along with the reduced $\psi = 0$ boundary conditions for the various modes of the nonlinear analysis, will be accurate at large enough Taylor number. This reduction of order and the simplicity of the basic vertical eigenfunction (compare the first term of B 3 with the whole thing) is important in making the nonlinear problem tractable.

$n = x_s Ta^{1/6}$	B_2	B_1	B_0
1	3.8	−7.13	−0.83
2	11.0	−20.5	5.36
4	21.9	−43.2	17.1
10	74.5	−147.4	68.7
20	247	−495	242
40	930	−1 861	926
100	5 380	−10 760	5 375
200	20 959	−41 918	20 953
400	82 855	−165 709	82 850
1000	514 521	−2*514 521	514 520
2000	2 055 189	−2*2 055 189	2 055 188

TABLE 1. Coefficients for the curly bracket term in (C 1).

Appendix C. Coefficients for the amplitude equation

Both coefficients C_1 and C_2 depend on x_s. A few values C_2 are illustrated below:

$$C_2 = \frac{\Gamma}{\sqrt{|\epsilon|Ta^{1/6}}}[0.49\,Pr - 7.34] \quad \text{at } x_s = 10Ta^{-1/6},$$

$$C_2 = \frac{\Gamma}{\sqrt{|\epsilon|Ta^{1/6}}}[0.99\,Pr - 5.40] \quad \text{at } x_s = 20Ta^{-1/6},$$

$$C_2 = \frac{\Gamma}{\sqrt{|\epsilon|T_a^{1/6}}}[-0.41\,Pr + 7.43] \quad \text{at } x_s = 100Ta^{-1/6}.$$

The numeric coefficients fluctuate periodically through order-one positive and negative values as x_s increases. When the Taylor number is large this coefficient is small.

C_1 is a function of x_s too. Its general form is

$$C_1 = -0.0809\,Pr^2Ta^{1/2} + (a_1Pr - a_2Pr^2)Ta^{1/4} - (2.61Pr^2 + 0.422Pr)Ta^{1/6} + \{B_2Pr^2 + B_1Pr + B_0\} + O(Ta^{-1/6}). \tag{C 1}$$

The values associated with the B's turn out to be more important than the a's because they grow with radius while the a's do not. Their dependence on radius is shown in table 1. Recall that x_s measures the base container radius for the local longitudinal rolls in units of layer thickness H. Inspection of this table reveals that a good approximation to the curly brackets of (C 1) for large n is obtained by writing, $\{\} \approx n^2(Pr-1)^2/2 = x_s^2Ta^{1/3}(Pr-1)^2/2$, so that

$$C_1 \approx \frac{\Gamma^2}{|\varepsilon|}\left[-0.0809Pr^2Ta^{1/2} + x_s^2Ta^{1/3}(Pr-1)^2/2 + O(Ta^{1/4})\right]. \tag{C 2}$$

When $C_1 = 0$ the physical effects represented by the first two terms on the right counteract each other. This occurs when $Ta \approx [6(Pr-1)x_s/Pr]^{12}$, which takes the value $[6(Pr-1)L/HPr]^{12}$ at the outer edge of the cylinder.

The a-terms in C_1 come from a peculiarity of our averaging procedure. They originate from resonances associated with the local average or projection of the second-order centrifugal buoyancy term onto the basic eigenfunction: $x\psi_1(x,z)T_{c2z}(z)$. Without the radius factor x, this would average (over an x-cycle) to zero. But as x is allowed to vary over the average, which starts at x_s, a non-zero result ensues. This may or may not be physically important. Resolution of its significance would require relaxation of the local rectilinear approximation. The terms retained are believed to capture the dominant physical effects.

REFERENCES

Barcilon, V. & Pedlosky, J. 1967 On the steady motions produced by a stable stratification in a rapidly rotating fluid. *J. Fluid Mech.* **29**, 673–690.

Brummel, N., Hart, J. E. & Lopez, J. M. 1999 On the flow induced by centrifugal buoyancy in a differentially heated rotating cylinder. *Theor. Comput. Fluid Dyn.* (submitted).

Boubnov, B. M. & Golitsyn, G. S. 1990 Temperature and velocity field regimes of convective motions in a rotating fluid layer. *J. Fluid Mech.* **219**, 215–239.

Chandrasekhar, S. 1961 *Hydrodynamic and Hydromagnetic Stability*. Oxford University Press.

Duncan, I. B. 1966 Axisymmetric convection between two rotating disks. *J. Fluid Mech.* **24**, 417–449.

Fernando, H. J. S., Chen, R.-R. & Boyer, D. L. 1991 Effects of rotation on convective turbulence. *J. Fluid Mech.* **228**, 513–547.

Hart, J. E. 1995 Nonlinear Ekman suction and ageostrophic effects in rotating flows. *Geophys. Astrophys. Fluid Dyn.* **79**, 201–222.

Hart, J. E. & Ohlsen, D. R. 1999 On the thermal offset in turbulent rotating convection. *Phys. Fluids* **11**, 2101–2107.

Homsy, G. M. & Hudson, J. L. 1969 Centrifugally driven thermal convection in a rotating cylinder. *J. Fluid Mech.* **35**, 33–52.

Homsy, G. M. & Hudson, J. L. 1971 Centrifugal convection and its effect on the asymptotic stability of a bounded rotating fluid heated from below. *J. Fluid Mech.* **48**, 605–624.

Hudson, J. L. 1968 Non-isothermal flow between rotating disks. *Chem. Engng Sci.* **23**, 1007–1020.

Julien, K., Legg, S., McWilliams, J. & Werne, J. 1996 Rapidly rotating turbulent Rayleigh–Bénard convection. *J. Fluid Mech.* **322**, 243–273.

Julien, K. & Knobloch, E. 1998 Strongly nonlinear convection cells in a rapidly rotating fluid layer: the tilted f-plane. *J. Fluid Mech.* **360**, 141–178.

Klinger, B. A. & Marshall, J. 1995 Regimes and scaling laws for rotating deep convection in the ocean. *Dyn. Atmos. Oceans* **21**, 227–256.

Koshmeider, E. L. 1967 On convection on a uniformly heated rotating plane. *Beitr. Physik Atmos.* **40**, 216–225.

Liu, Y. & Ecke, R. E. 1997 Heat transport scaling in turbulent Rayleigh–Bénard convection: Effects of rotation and Prandtl number. *Phys. Rev. Lett.* **79**, 2257–2260.

Liu, Y. & Ecke, R. E. 1998 Experimental investigation of turbulent rotating Rayleigh–Bénard convection. *J. Fluid Mech.* (submitted).

Sakai, S. 1997 The horizontal scale of rotating convection in the geostrophic regime. *J. Fluid Mech.* **333**, 85–95.

Veronis, G. 1966 Motions at subcritical values of the Rayleigh number in a rotating fluid. *J. Fluid Mech.* **24**, 545–554.

Veronis, G. 1968 Large amplitude Bénard convection in a rotating fluid. *J. Fluid Mech.* **31**, 113–139.